

Review

Synthesis of conducting nanowires

S. BANERJEE

Department of Physics, University of Calcutta, Calcutta 700 009, India

A. DAN, D. CHAKRAVORTY

Indian Association for the Cultivation of Science, Calcutta 700 032, India

E-mail: mlsdc@mahendra.iacs.res.in

Work reported on the synthesis of nanowires of different metals/alloys and semiconductors respectively in recent years is reviewed. The methods used mostly belong to one of the following categories: chemical, electrodeposition, physical and filling of carbon nanotubes. Electrical properties investigated for some of these nanowires indicate quantum mechanical effects to be present. Nanodevice fabrication using doped semiconducting nanowires has also been reported. © 2002 Kluwer Academic Publishers

1. Introduction

Synthesis and characterization of nanostructured materials have been a major area of research activities in the last decade or so [1–3]. Many interesting problems have been thrown up because of unusual properties exhibited by these materials [4–6]. Nanoscale electronics is a fast developing field and is predicted to play a significant role in future device technology [7]. Useful and interesting properties have been reported in the case of nanowires of metallic alloys [8] and semiconductors [9]. In nanodevice fabrication quantum dots will figure extensively. For interconnection of these nanodevices metallic nanowires will be needed a great deal. All these have led to intense research efforts in the last few years to develop techniques to grow nanowires of metals and semiconductors. In this article we review briefly the work reported in respect of nanowire fabrication for metals and semiconductors.

Several physical and chemical techniques have been exploited for the above purpose. The subsequent paragraphs delineate the results obtained.

2. Chemical route

This approach involves selecting suitable precursor chemical(s) which was subjected to heat treatment under different atmospheric conditions.

Heath *et al.* [10] applied a *solution phase synthesis* for preparing single crystal Ge quantum wires. GeCl_4 , phenyl- GeCl_3 and dry hexane mixture was reduced by metallic Na dispersion in toluene at temperature 275°C and pressure 100 atm. Nanowires having diameter range 7–30 nm and length upto $10\ \mu\text{m}$ were synthesized by this method. Wire diameter could be reduced to 5 nm, by using excess Na in the reaction. Growth morphology and reaction mechanisms were explained.

Huber *et al.* [11] used the *pressure injection technique* for preparing nanowire arrays of metals (In, Sn

and Al) and semiconductors (Se, Te, GaSb and Bi_2Te_3) within the channels of anodic alumina membranes. The nanochannel alumina and the materials were sealed in a metal ampoule and placed in a reactor of high pressure and high temperature injection apparatus. At an elevated pressure molten material was injected within the channels, overcoming the surface tension force.

Trentler *et al.* [12] synthesized crystalline InP, InAs and GaAs fibers (widths 10–150 nm and lengths upto several microns) using simple *organometallic reactions* conducted at low temperatures in hydrocarbon solvents. Toluene solution of tri-tert-butylindane precursor with 10 mol% PhSH was stirred at room temperature and heated to reflux at 111°C in heating mantle. Xray and TEM analysis of the resulting precipitate revealed the existence of InP fibers. For InAs 1, 3-diisopropyl-benzene along with excess AsH_3 were used. 1, 3-diisopropylbenzene solution of tri-tert-butylgallane was chosen for GaAs fiber production. Formation of such fibers was explained by solution-liquid-solid growth mechanism.

Silicon nanowires with diameters ranging from 4–5 nm and lengths of several microns were synthesized by Holmes *et al.* [13] by a *supercritical fluid solution-phase approach*. Dodecane-thiol capped gold nanocrystals (2.5 nm in diameter) were dispersed in supercritical hexane with diphenylsilane. At 500°C and pressure of 200 and 270 bar respectively, diphenylsilane decomposed to Si atoms which dissolved in the Au nanocrystals until reaching a Si-Au alloy supersaturation, when Si was expelled from the nanocrystal as a crystalline nanowire. Orientation of nanowires depended on reaction pressure. The wires formed at 200 bar were oriented along (100) direction whereas at 270 bar they were oriented along (110) direction. Fig. 1a and b show the transmission electron micrographs of Si nanowires formed at 200 and 270 bar respectively. Room temperature optical absorption was studied for

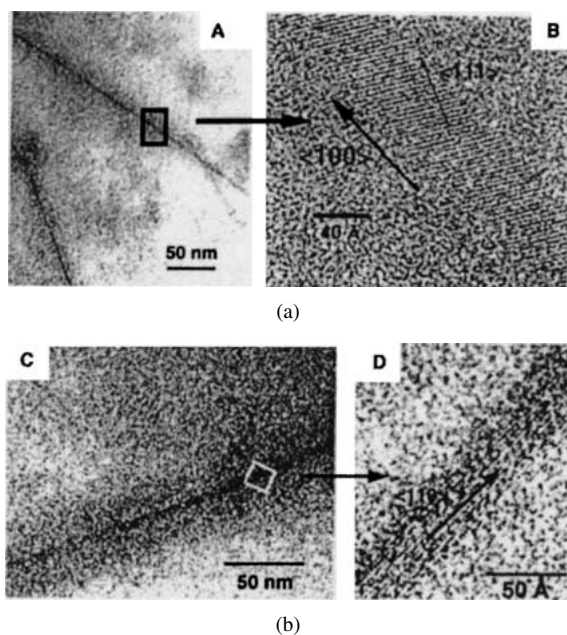


Figure 1 Transmission electron micrograph of Silicon nanowires grown by supercritical fluid solution-phase approach [13]. (a) 500°C in hexane at a pressure of 200 bar. (b) 500°C in hexane at a pressure of 270 bar. (Reprinted with permission from J. D. Holmes, K. P. Johnston, R. C. Doty and B. A. Korgel, *Science* **287** (2000) 1471. Copyright (2000) American Association for the Advancement of Science.)

Si nanowires suspended in hexane. Absorption edge was blue shifted from the bulk indirect gap of 1.1 eV and distinct optical transition was observed. The $\langle 100 \rangle$ oriented wires exhibited higher exciton energy than the $\langle 110 \rangle$ wires. In photoluminescence spectra $\langle 100 \rangle$ wires exhibited a single peak at 3.75 eV with a weak shoulder shifted to 1.9 eV. The $\langle 110 \rangle$ wires had 3 peaks at 3.35, 2.9 and 2.55 eV. Optical properties were explained by quantum confinement effects.

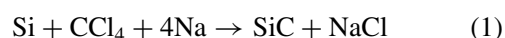
Han *et al.* [14] prepared Au, Ag and Pt nanowires using hexagonal *mesoporous silica SBA-15* as template. SBA-15 with a hexagonal array of 1D channels of nanometer dimension, were obtained using Plunoric P123 and Tetraethyl Orthosilicate under acidic condition [15]. Calcinated SBA-15 were immersed in respective salt solution (HAuCl_4 , $\text{Pt}(\text{NH}_3)_4(\text{NO}_3)_2$ and AgNO_3) and subsequently reduced in H_2 atmosphere at 393, 593 and 623 K respectively. Nanowires of diameter ~ 7 nm and length 50 nm–1 μm were grown within the channels of SBA-15.

A novel method for *surfactant-assisted growth* of crystalline Copper Sulfide nanowires was reported by Wang *et al.* [16]. A Chloroform solution of Sodium bis(2-ethylhexyl) sulfosuccinate (NaAOT) was spread on rough oxidized copper surface (copper grid or block). Dried surface was kept at H_2S atmosphere for 12 h at room temperature. Straight, uniform wires with high density and large aspect ratio (diameter of minimum 10 nm and length of maximum 30 micron) were formed from copper surface. HRTEM revealed that nanowires exhibited core/shell structure, with monoclinic core Cu_2S and a tetragonal shell $\text{Cu}_{1.96}\text{S}$. Fig. 2 shows a typical transmission electron micrograph for Cu_xS nanowires [16].

Meng *et al.* [17] synthesized SiC nanowires by *carbothermal reduction* of SiO_2 xerogels containing car-

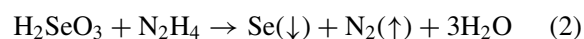
bon nanoparticles. Wires were formed by *carbothermal reduction* at 1650°C for 1.5 h and followed by heating to 1800°C and holding for 30 min. in flowing Ar atmosphere. TEM, SAED, and EDX showed that wires were composed of 10–25 nm diameter crystalline b-SiC cores surrounded by amorphous SiO_2 sheathes with outer diameters in the range 20–70 nm. Also bare SiC nanowires (15–30 nm diameter) were formed by carbothermal reduction at 1650°C for 2.5 h in flowing Ar atmosphere. During carbothermal reduction SiO and CO gas was generated. Flowing Ar-atmosphere, produced lower super-saturation of SiO gas, favoring one dimensional growth of whiskers.

Hu *et al.* [18] prepared Silicon Carbide (3C-SiC) nanowires (diameters 15–20 nm and lengths 5–10 micron) by *reduction-carburization* route. Appropriate amount of Si powder, CCl_4 and metallic Na were heated in titanium alloy autoclave at 700°C for 10–48 h. Following reaction step was proposed:



The product was treated with dilute $\text{HF} + \text{HNO}_3$ to remove unreacted Si. Then it was heated to 600°C for 3 h and further treated with dilute HF and washed with distilled water to get a gray-white product. Formation of SiC-nanowires was explained by vapor-liquid-solid (VLS) mechanism. Raman spectra were recorded with a backscattering configuration. Two broadened bands at 776 cm^{-1} and 954 cm^{-1} were attributed to the TO and LO phonon at the gamma point of cubic SiC respectively. Both bands were shifted by $19\text{--}20\text{ cm}^{-1}$ towards lower energy. Room temperature spectra showed a strong peak at 448 nm for excitation at 385 nm.

Gates *et al.* [19] prepared defect free trigonal Se nanowires (diameter 10–30 nm) by a *solution phase approach*. Colloidal dispersion of Se was formed, by refluxing Selenious acid (0.04 M) with excess Hydrazin (0.75 M) at 100°C.

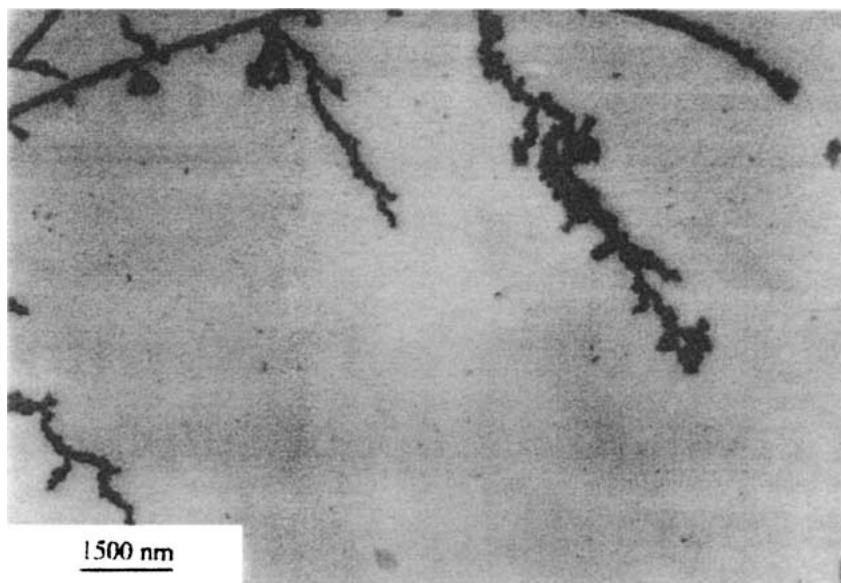


Nanowires were formed on aging the dispersion at room temperature in darkness. Diameters of wire were reduced to 10 nm when solution was refluxed at $\sim 90^\circ\text{C}$.

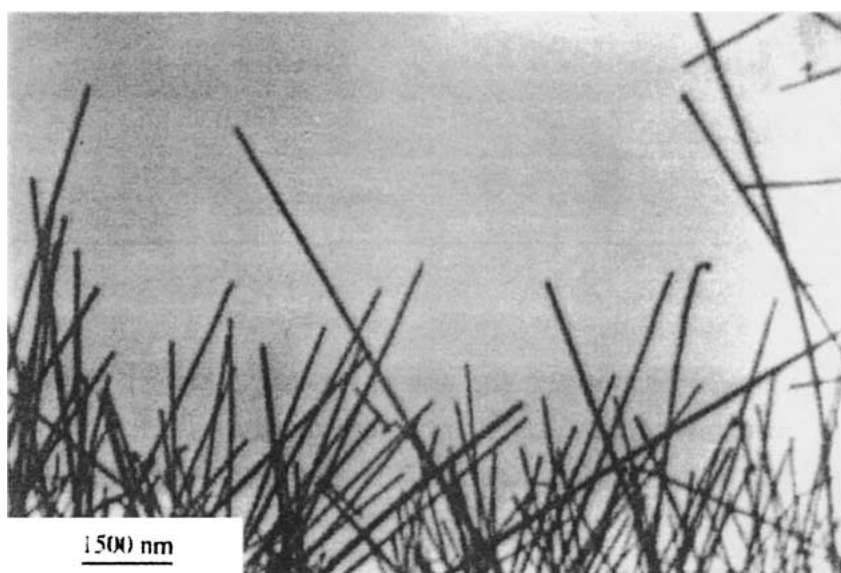
A novel *supercritical solution phase approach* was utilized by Coleman *et al.* [20] to fill 5 nm diameter pores of hexagonal mesoporous silica with silicon nanowires. Wires were formed by degrading diphenylsilane in a high pressure reaction cell at 500°C and at a pressure of 375 bar.

Polymer controlled growth of CdS nanowires was investigated by Zhan *et al.* [21] Cd^{2+} containing polyacrylamide gel was treated with thiourea solvothermally in ethylenediamine at 170°C. After 10 days in autoclave a yellow product was obtained. Single crystal CdS nanowires of length upto 100 μm and diameters about 40 nm were fabricated. Large aspect ratio was attributed to the presence of the polymer medium.

Bjorholm *et al.* [22] synthesized polythiophene nanowires by collapsing a monolayer of amphiphilic polythiophene on a Langmuir-Blodgett (LB)-trough.



(a)



(b)

Figure 2 Transmission electron micrograph of Cu_xS nanowires grown by surfactant pretreatment [16]. (Reprinted from Suhua Wang and Shihe Yang, *Chemical Physics Letters* **322** (2000) 567. Copyright (2000), with permission from Elsevier Science).

Monolayers spontaneously folded into wire-like structures when compressed beyond the collapse point. AFM images revealed that nanowires of lengths \sim microns, widths of 60 nm and heights 10–15 nm were formed by this process. Room temperature resistivity of the nanowires was found to be $2.5 \times 10^{-4} \Omega\text{-cm}$. Resistivity data of iodine doped nanowires in the temperature range 300–4.2 K exhibited the activated behavior following the relation

$$\rho = \rho_0 \exp\left(\frac{T_0}{T}\right)^\alpha \quad (3)$$

α was found to be 0.5 consistent with the cermet systems.

Table I summarizes the various systems of nanowires synthesized by chemical route.

TABLE I Nanowires synthesized by chemical route

Material	Diameter (nm)	Technique	Reference
Ge	7–30	Solution phase synthesis	[10]
In, Sn, Al Se, Te, GaSb Bi ₂ Te ₃	200	Pressure injection	[11]
InP, InAs, GaAs	10–150	Organometallic reaction	[12]
Si	4–5	Supercritical fluid solution-phase	[13]
Au, Ag, Pt	7	Mesoporous silica template	[14]
CuS	10	Surfactant assisted growth	[16]
SiC	10–30	Carbothermal reduction of SiO ₂	[17]
SiC	15–20	Reduction carburization	[18]
Se	10–30	Solution phase	[19]
Si	5	Supercritical solution phase	[20]
CdS	40	Polymer controlled growth	[21]
Polythiophene	60	Collapsing polymer	[22]

3. Electrodeposition route

Electrodeposition is a relatively simple and inexpensive method. Nanowires of large aspect ratio can be grown within pores of nuclear track etched polymer membranes, mica or in pores of self-ordered nanochannel materials (anodized Al₂O₃, Glass). Wires are mechanically stable within the templates and they are easy to handle. As the wires are aligned in many cases, anisotropic physical properties can be studied.

Sun *et al.* [23] used track etched mica wafers for electrodeposition. Diamond shaped nanopores with lateral dimensions as small as 30 nm was fabricated by nuclear track etching in 5 μm thick, single-crystal muscovite mica wafers. Particle tracks were created by exposure to 6 MeV α particles from a 100 μCi Cf²⁵² source. Nickel nanowire arrays were synthesized by electrodeposition into the nanopores using a solution of NiCl₂ · 6H₂O, Ni(H₂NSO₃)₂ · 4H₂O, H₃BO₃ buffered to pH 3.4 at a potential of -1.0 V (Ag/AgCl). The hysteresis loops for the Ni nanowire arrays exhibited strong shape anisotropy due to the nanowire geometry. For magnetic field applied parallel to the wires, coercivity increased with decreasing effective diameter, reaching a value of 800 Oe at wire diameter of 30 nm. The squareness, (ratio of remanence and saturation magnetization) decreased with increasing wire diameter.

Evans *et al.* [24] synthesized Co–Ni–Cu/Cu multilayered nanowires by *electrodeposition* using nanoporous aluminum oxide membranes. Commercially available anodic aluminum oxide membranes of thickness 60 μm , with pore diameter 20 nm and pore density 10¹⁰ cm⁻², were used for these experiments. Multilayered nanowires were prepared by switching between a potential of -1.6 V relative to the saturated calomel reference electrode, at which a ferromagnetic Co–Ni–Cu alloy was deposited, and -0.2 V, at which pure Cu was deposited.

Fasol *et al.* [25] used the cleaved edge of a molecular beam epitaxy (MBE) grown 4-nm quantum well to deposit metal nanowire by *electroplating technique*. A series of InGaAs and InAlAs layers of nanometer thickness were deposited by MBE onto an undoped InP substrate. Modulation doped structure caused electron to drop from the heavily doped InAlAs layer into a 4-nm InAs layer, which acted as conducting template. For electrodeposition citrate-complexed nickel-iron solution of pH ~ 4.5 was chosen. AFM image confirmed that 20 nm thin permalloy wires were grown within the template.

Xu *et al.* [26] synthesized CdSe nanowire arrays in porous anodic aluminum oxide (AAO) templates (pore diameter ~ 20 nm and length ~ 28 micron) by *direct-current electrodeposition*. CdCl₂ solution saturated with elemental Se in dimethyl sulfoxide (DMSO) was used as electrolyte. CdSe was cathodically deposited between the Ag/AAO working electrode and Pt counterelectrode by applying a constant dc density 0.85 mA/cm² for 30–60 min. Nanowires of uniform length (~ 6 micron), diameter (~ 20 nm) were grown with hexagonal symmetry.

Electrochemical growth method was exploited to synthesize conducting polymer nanowires on gold

electrodes modified with self-assembled monolayers (SAMs) of well-separated thiolated cyclodextrins in an alkanethiol “forest” [27]. Thiolated aniline monomer was anchored to the surface within the cyclodextrin cavity and formed an initiation point for polymer wire growth.

A polymer was used as a template to grow metallic nanowires [28]. Polyvinyl alcohol film subjected to a two-stage treatment viz., in ammonium persulphate and Pyrrole solutions respectively was the medium in which silver nanowires of dimension ~ 2 nm and length ~ 2 mm were grown by an electrodeposition method.

Pores of heat treated silica gel were used for growing silver nanowires by electrodeposition technique [29]. The diameter was of the order of 40 nm and length ~ 0.3 mm. By disrupting the nanowire with an electrical pulse a staircase current-voltage characteristic was observed.

As a variant to the above mentioned technique a suitably chosen glass (composition 40 Li₂O, 12CaO, 3Al₂O₃, 45 SiO₂) was ion exchanged (Li⁺ Δ Ag⁺) by dipping a sample of cross-section ~ 0.3 cm² and thickness ~ 1.3 mm in a molten bath of AgNO₃ at 573 K for a duration of 11 hours. After washing the ion-exchanged sample by distilled water, silver paste electrodes were applied on two opposite faces. The sample was heated to a temperature ~ 600 K so that the resistance was $\sim 10^6$ ohms. A dc voltage of 10 volts was applied across the specimen. This brought about formation of silver nanowires [30]. Fig. 3a is the transmission electron micrograph for the nanowire produced and Fig. 3b is the corresponding electron diffraction pattern. The latter confirms the presence of silver phase. The diameter of the wire is ~ 20 nm. In Fig. 4 is shown the voltage-current characteristics of the nanocomposite containing silver nanowires at two different temperatures. The symmetrical nature of the linear behaviour substantiates the ohmic nature of the metal nanowires.

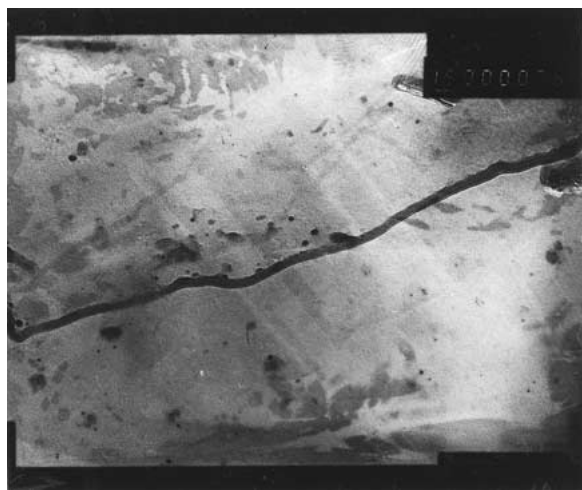
Cao *et al.* [31] fabricated array of cobalt nanowires encapsulated in Polyaniline nanotubules supported inside the pores of alumina membranes (second-order template). First of all aniline was polymerized within the pores of alumina membranes. Then CoSO₄ · 7H₂O and H₃BO₃ solution was electrodeposited within polyaniline nanotubules.

Sapp *et al.* [32] used Bi³⁺/HTeO₂⁺ solution for synthesis of bismuth telluride (Bi₂Te₃) nanowires within the pores of anodic alumina membranes by *galvanostatic deposition* at current density 3.5 mA/cm². Nanowires of diameter 280 nm and lengths ~ 60 μm were prepared by this process.

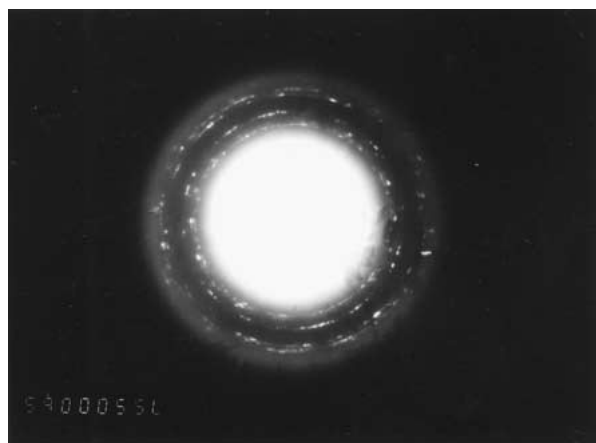
In Table II we summarize the various systems of nanowires grown by the electrodeposition technique.

4. Physical route

Kondo *et al.* [34] synthesized suspended gold nanowires in an ultra high vacuum-TEM (vacuum level 3×10^{-8} Pa) with the *electron beam thinning technique*. A gold (011) film of thickness 3–5 nm was cleaned previously by electron beam irradiation and subjected to intense electron beam (200 kV, 500 A/cm²). Further thinning by weaker electron beam



(a)



(b)

Figure 3 (a) Transmission electron micrograph of Silver nanowires grown in an ion-exchanged glass of composition $40\text{Li}_2\text{O}$, 12CaO , $3\text{Al}_2\text{O}_3$, 45SiO_2 by electrodeposition method [30]. (b) Electron diffraction pattern of Fig. 3a [30].

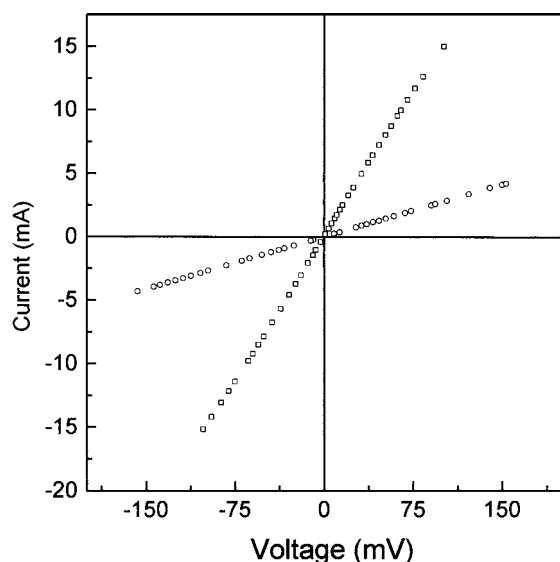


Figure 4 Voltage-current characteristic of a glass nanocomposite containing silver nanowires of diameter 20 nm [30].

($10\text{--}50\text{ A/cm}^2$) resulted in new structures with diameters $0.6\text{--}1.5\text{ nm}$ and length $3\text{--}15\text{ nm}$. High resolution electron microscopy revealed that the wires had multishelled structure composed of coaxial tubes with

TABLE II Nanowires prepared by electrodeposition route

Material	Diameter (nm)	Technique	Reference
Ni	30	Electrodeposition in nanopores of track etched mica wafer	[23]
Co-Ni-Cu/Cu multilayer	20	Electrodeposition in nanopores of Al_2O_3 membrane	[24]
Ni_3Fe	20	Electroplating in quantum well structure InGaAs-InAlAs	[25]
CdSe	20	Anodic Al_2O_3 template	[26]
Conducting polymer	20	Combined electrodeposition and mechanical break junction method	[33]
Ag	2	Polyvinyl alcohol films as template	[28]
Ag	40	Silica gel pores as template	[29]
Co	200	Electrodeposition within polyaniline nanotubes	[31]
Bi_2Te_3	280	Anodic Al_2O_3 template	[32]

helical atom rows coiled around the wire axis. A structure model of n -fold helix composed of a tube with a triangular network was proposed. TEM image simulations based on this structure were compared with the experimentally observed images. A fairly good agreement showed that the difference between the numbers of atom rows in outer and inner shells was seven, resulting in magic shell closing numbers.

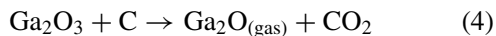
Bai *et al.* [35] synthesized GeO nanowires by *physical evaporation* method. A hot pressed pellet of Ge powder mixed with 8 wt% Fe powder was used as target. The plate was heated inside a quartz tube to 820°C under flowing Ar at a pressure of about 200 Torr. The flow rate was controlled by mass flow controller. Presence of GeO nanowires of diameter ranging from $15\text{--}80\text{ nm}$ was observed under TEM. The spotty pattern in electron diffraction pattern indicated that GeO_2 single crystals had hexagonal structure.

Yu *et al.* [36] used less expensive and simple *physical evaporation* technique to synthesize silicon nanowires of uniform diameter around 15 nm. Asymmetrical Transverse optical (TO) Raman peak was shifted from 522 cm^{-1} of crystalline Si to 509 cm^{-1} of SiNW. This was explained by phonon strain field, caused by, various structural imperfections present in nanowires. Photoluminescence (PL) spectra was recorded at room temperature using 325 nm excitation light from Dye laser. Two distinct peaks at about 2.4 and 2.95 eV were observed. This was attributed to an amorphous overcoating layer of silicon oxide as revealed from transmission electron micrograph.

Yan *et al.* [37] synthesized amorphous silicon nanowires (a-SiNW) on heavily doped n type Si (111) chip. A thin 40 nm Ni was deposited on Si substrate. This substrate was kept at 950°C under an Ar/ H_2 atmosphere for duration of about 1 h. High resolution transmission electron microscopy with energy dispersive spectroscopy revealed that nanowires of average diameter of 20 nm and length of up to a tens of microns were composed mainly of silicon. Growth of nanowires was explained by solid-liquid-solid (SLS) mechanism. At about 930°C Si_2N eutectic liquid alloy droplets were formed over the Si substrate. Due to high solubility more

Si atoms were dissolved and the liquid phase became supersaturated resulting in growth of nanowires. Cross sectional SEM confirmed the SLS mechanism.

Peng *et al.* [38] used *hot filament chemical vapor deposition* technique to synthesize bulk-quantity single crystal GaN nanowires. This method required neither a metal catalyst nor the effect of nanometer sized confinement such as carbon nano tubes or porous alumina as template. A solid source (pressed tablet of Ga₂O₃ and C powders) was heated by tungsten filaments at 900°C in NH₃ atmosphere (flow rate 100 sccm) of total pressure of 200 Torr. Highly pure nanowires of diameter 5–12 nm were grown on graphite substrate placed below the filaments. They had hexagonal wurzite structure, grown perpendicular to {101 $\bar{1}$ } plane. Two step reaction mechanisms were proposed.



Monoclinic Gallium oxide (β -Ga₂O₃) nanowires were synthesized by Choi *et al.* [39] by *DC arc discharge* of GaN powders with small amount of transition metals (Ni/Co and Ni/Co/Y) in argon and oxygen mixture at a pressure of 500 Torr. GaN powder was placed in the hole of graphite anode and 55–65 A current was applied across the electrodes for 5–6 Sec. Web like structure consisting of nanowires of length $\sim 100 \mu\text{m}$ and diameter $\sim 30 \text{ nm}$ was analyzed by TEM and HRTEM. A catalyst-assisted step growth mechanism was proposed in explaining the formation of wires.

Laser ablation seems to be the most promising for synthesizing SiNWs because this method can produce free-standing nanoscale materials in high yield and purity with controllable experimental conditions. Sufficient quantities of nanowires are useful for detailed studies of their physical properties and potential applications.

Silicon nanowires were prepared by Zhang *et al.* [40] by using a high temperature *laser ablation* technique. A Si target placed inside an argon gas filled quartz tube was vaporized at temperature 1200°C by an excimer laser producing pulse energies of 400 mJ of duration 34 nS. A sponge-like web consisting of Si nanowires was formed on the inner wall of quartz tube surrounding the tip of copper cold finger. Crystalline nanowires having diameter ranging from 3–43 nm and length up to a few hundred microns were observed under TEM. Twins and stacking faults were observed in the Si core of nanowires. Raman scattering from the nanowires showed an asymmetrical peak at 521 cm⁻¹ with a FWHM of 12 cm⁻¹ and extended tail at low frequencies.

Tang *et al.* [41] used *laser ablation* method for preparing Si nanowires from a target of SiC powder mixed with 10 wt% SiO₂ powder. A KrF excimer laser beam (248 nm) with 400 mJ per pulse was used for ablation. Two layers of sponge-like webs—a yellow web a green web were deposited on the walls of the tube. From HRTEM image co-existence of SiC nanoparticles with crystalline Si nanowires was confirmed.

TABLE III Nanowires synthesized by physical route

Material	Diameter (nm)	Technique	Reference
Au	0.6–1.5	Electron beam thinning	[34]
GeO	15–80	Evaporation	[35]
Si	15	Evaporation	[36]
a-Si	20	Evaporation	[37]
GaN	5–12	Hot filament chemical vapour deposition	[38]
β -Ga ₂ O ₃	30	Dc arc discharge	[39]
Si	3–43	Laser ablation	[40]
Si	14	Laser ablation (target SiC)	[41]

General synthesis of wide range single crystal binary and ternary III-V, II-VI and IV-IV, compound semiconductor nanowires was reported by Duan *et al.* [42] Laser-assisted catalytic growth (LCG) method was exploited for preparing nanowires of minimum diameter $\sim 3 \text{ nm}$. Growth of nanowires was explained by vapor-liquid solid growth mechanism.

Table III lists the physically deposited nanowires of different systems.

5. Carbon nanotube filling

Liang *et al.* [43] reported the *filling of carbon nanotubes* with Ni by chemical vapor deposition of C₆H₆ at 1000°C for 1 h over Raney-Ni catalyst. TEM study revealed three types of structures—bamboo shaped with every head compartment filled with Ni particles, nanotubes with end compartment filled with needle shaped Ni and straight nanotubes encapsulated completely with Ni crystal. Different growth mechanisms were proposed for nanowire filling.

Sinha *et al.* [44] used aluminophosphate molecular sieves AIPO-5 and AIPP-31, for *filling the nanotubes* with Co nanowires. The support materials were stirred with cobalt nitrate solution at 353 K and then dried. Powered sample was subjected to a treatment at 973 K under acetylene gas flow. A weak metal-support interaction was proposed to explain the nanowire filling.

Molecular nanowires inside single-walled carbon nanotubes were prepared by Kiang *et al.* [45] Bi was drawn into the nanotubes by *capillary attraction*, where single crystal nanowires were formed. In gas phase reaction, Bi metal was incorporated in the composite anode and vaporized with carbon and cobalt in Helium atmosphere. In solid phase reaction, nanotube soot with excess Bi nanoparticle was heated in air at 400 C for 30 minute, which resulted in opening up of nanotubes and subsequent filling. But solution phase method was proved to be most efficient (more than 30% of tubes can be filled) yielding nanowires of high aspect ratio. Chemically cleaned Carbon nanotube soot was stirred in Bi(NO₃)₃ in HNO₃ solution. After centrifugation, the precipitate was washed, dried in H₂ atmosphere. Nanowires of diameter 1 nm were prepared by this process.

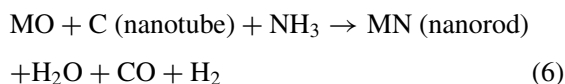
In general strong electronic interaction between host carbon nanotube and filling metal may yield metallic carbides. Incorporation is often found to be similar to that in graphitic intercalation compounds, especially in

TABLE IV Nanowires synthesized by filling of carbon nanotubes

Material	Diameter (nm)	Technique	Reference
Ni	4	Chemical vapour deposition	[43]
Co	25–28	Aluminophosphate molecular sieves	[44]
Bi	1	Capillary attraction	[45]
GaN	14.9	Reaction with gaseous oxide in NH ₃	[46]

case of alkali metal intercalation. To reduce the complications several workers proposed to fill Boron nitride nanotubes with metal atoms [46, 47]. Boron nitride nanotubes behaves like ideal noninteracting hosts for metal inside. Boron Nitride is a stable insulator with band gap 5.5 eV, and is less polarizable than metals and semimetals.

Han *et al.* [48] synthesized 14.9 nm diameter GaN nanorods by reacting gaseous metal Oxide (MO) with carbon nanotubes in an NH₃ atmosphere.



In Table IV we summarize the different systems for which nanowires were fabricated by the filling of carbon nanotubes.

Berry *et al.* [49] fabricated uniform, high-density GaAs and InAs nanowires in porous *nano channel glass* (NCG). Me₃Ga, Me₃In and iso-Bu₃In were used as precursors. NCG was submerged in liquid precursors at ambient temperatures for several hours to fill the channels via capillary action. Further reaction with arsine (AsH₃) and subsequent annealing at 400–500°C yielded polycrystalline GaAs and InAs wires with crystallite sizes of approximately 50–130 Å. At higher temperatures, the InAs wires exhibited linear increase in porosity and grain size, whereas GaAs wires maintained a uniform, smooth texture.

6. Electrical property

Bezryadin *et al.* [50] measured the electrical conductivity of Mo-Ge alloy nanowires (thickness 5.5 ± 1 nm) synthesized by *sputtering* alloy of amorphous Mo₇₉Ge₂₁ over free-standing carbon nanotubes. Electrodes were prepared on a single nanowire by optical lithography and reactive ion etching process. It was found that the wires were superconducting only if their normal-state resistance (R_N) was lower than the quantum resistance ($R_q = h/2e^2 \sim 6.5$ k-ohm), and insulating otherwise. The insulating and superconducting properties became stronger when the difference $|R_N - R_q|$ increased. The difference between the superconducting and insulating samples became more pronounced at low temperatures, which suggested that the transition was driven by quantum fluctuations. Such type of quantum localization transition was called a dissipative phase transition (DPT). At weak dissipation, the tunneling of phase slips was dominant and destroyed superconductivity.

Coulomb blockade (CB) was observed by Davydov *et al.* [51] in Al/Aluminum oxide/Ni nanowire single tunnel junction arrays formed by ac electrochemical deposition in porous aluminum oxide nanotemplates. The aluminum oxide barrier layer, which consisted of tunnel junctions were varied from 7–28 nm. Tunneling spectra $G(V) = dI/dV$ exhibited zero bias dips. Tunneling conductance was quite independent of temperature above some critical bias voltage with the variation $G \sim V^\alpha$, where $\alpha \sim 0.45$. This dependence was attributed to electron-electron interactions in the disordered metal wires. Metal wires connected to tunnel barrier gave rise to additional tunnel conductivity G (eV) = $G_0 [1 + (eV/\Delta)^{1/2}]$, where Δ was degree of disorder. Theoretical prediction for CB in ID system was helpful in explaining the experimental data [52, 53]. CB was dominated by the leads with substantial tunneling conductance, when R_1 was small compared to Quantum resistance $R_Q = h/2e^2 = 12.9$ K-Ohm, but total lead resistance remained larger than R_Q where $R_1 = C_j R_0 / C_0$; C_0 and R_0 were the leads capacitance and resistance per unit length, C_j was the junction capacitance. C_j was estimated to be 3×10^{-18} F, R_0 was measured to be 30 and 8 k-Ohm/ μm at 4.2 K for 12 nm and 16 nm diameter samples. Experimental data were fitted with theoretical proposed value of first derivative of tunnel conductance with V_c as parameter.

$$(d^2 I/dV^2) R_0 V_c = [4(V/V_c)^3]^{-1/2} \exp(-V_c/4V) \quad (7)$$

where $V_c = e^3 R_0 / C_0 \hbar$. Thus C_0 was estimated to be $\sim 10^{-17}$ F/ μm and R_1 to be ~ 1 K-Ohm. Stray capacitance arising from inter electrode and inter wire configuration did not affect CB due to high lead resistance which effectively decoupled tunnel junction.

D. Natelson *et al.* [54] measured electrical resistance and conductance fluctuations of continuous AuPd alloy wires with diameters as small as 5 nm and lengths greater than 1 micron in the temperature range 300–4.2 K by 4 terminal bridge technique. Resistance of the wires decreased with decrease in temperature followed by an increase at low temperature for the 5 nm and 20 nm width samples (below 80 K and 12 K respectively). The overall resistance change with temperature was reduced for smaller wire diameter, consistent with boundary scattering affecting the elastic mean free path in smallest wires. Increase of resistance for $T \rightarrow 0$ could be explained by electron-electron interaction causing a decrease of density of states near Fermi level. Diffusion motion of electron enhanced their interactions with the relevant length scale (L_T). The resistance rise was explained as

$$\frac{\Delta R}{R_0} = \frac{1}{\sqrt{2}} (4 - 1.5F) \frac{e^2 R_0}{hL} L_T \sim T^{-1/2} \quad (8)$$

where F ($0 < F < 1$) was a screening parameter, R_0 the sample resistance at a reference temperature. Appreciable amount of resistance noise was recorded for low temperature regime and small sample diameter. Universal conductance fluctuation (UCF) was caused due to phase difference between the carrier trajectories. At

low temperature thermal smearing was reduced causing an increase of electron phase coherence length and subsequently leading to growing UCF. The resistance data at 4.2 K as a function of perpendicular magnetic field was explained by one dimensional weak localization (WL) where applied magnetic field broke the time reversal symmetry causing interference between pairs of time-reversed trajectories leading to correction of conductivity. The MR data were fitted with Nyquist time as fitting parameter.

Kanjanachuchai *et al.* [55] fabricated nanowires from a modulation-doped Si/Si_{0.7}Ge_{0.3} heterostructure which showed coulomb blockade at very low temperatures due to single-electron charging of multiple islands. It was believed that threading dislocations were the origin for the formation of Coulomb islands in the wires. A nonblocked behavior was also seen in some wires. This was explained by a combination of incomplete tunnel barrier formation and leakage currents. The leakage manifested itself in the form of B_2 dependence in magnetoresistance measurements. Source of leakage was found from the substrate.

Transport measurements were carried out by Chung *et al.* [56] on 15–35 nm diameter Si nanowires (SiNW). Nanowires were synthesized by chemical vapor deposition from SiH₄/He gas via Au or Zn particle nucleated Vapor-liquid-solid growth at 440°C. A three terminal device was fabricated using Al and Ti/Au electrodes connected with nanowires. All devices prior to annealing showed I-V characteristics of back-to-back Schottky type diodes. Gate voltage dependent nonlinear I-V characteristics with current \sim pA (at $V_{\text{bias}} = 4$ V) were obtained for Au-SiNW and Zn-SiNW. Increase of conductance by $> 10^3$ of Zn-SiNW devices upon annealing at 550°C, was attributed to effect of Al electrode/NW contacts. For Au-SiNW device (Ti/Au electrodes) annealing at 750°C increased the current (at $V_{\text{bias}} = 4$ V) by 10^4 . Also annealed device showed metallic like conductance without any gating effect. Increased conductance was explained by both doping and decreased contact resistance.

The physical properties of a one dimension (1-D) metal are different from metals with a Fermi liquid of electron, due to strong electron-electron correlation in 1-D. Electron-electron coulomb repulsion decreases the energy density of states near Fermi level. In the absence of a long range interaction an 1-D electron liquid (so called “Luttinger Liquid” [57] is formed, while long-range coulomb interaction yields a 1-D Wigner crystal [58]. In coulomb blockade systems the tunneling transparency of a barrier vanishes due to electron-electron interaction, resulting in a power law zero-bias anomaly for the conduction [59, 60].

Zotov *et al.* [61] observed electrical transport in long InSb degenerate semiconductor nanowires over a temperature range 1.5–350 K. Wires (diameter ~ 50 Å, length 0.1–1 mm) were produced by filling InSb within the pores of natural asbestos at a pressure of 15 kbar at 550°C. The zero-field electrical conductance (G) showed the temperature dependence as $G \sim T^\alpha$ with $\alpha \sim 4.0$. At 1.8 K current-voltage characteristic followed the power law $I \sim V^\beta$; $\beta \sim 4.4$ for seven or-

ders of current variation. The InSb wire with diameter $d = 5$ nm and effective carrier mass $m^* = (0.014-0.2) m_e$, the energy separation between 1st and 2nd quantum level exceeded the energy corresponding to experimental temperature range. Thus quantum wires consisted of a few quantum conduction channels. The transport properties of individual wires were determined by impurities and weak links. Every wire was approximated by a system of Luttinger liquid (LL) drops connected in series by weak links of density 10^3-10^4 cm⁻¹. Power law behavior for $G(T)$ and $I(V)$ was explained by theoretical model of drops of LL in series connected by weak links.

Gurevich *et al.* [62] investigated the coulomb drag current in the ballistic transport regime in a nanowire by a ballistic current in a nearby wire. Giant oscillation in the drag current was studied as a function of gate voltage or chemical potential. Giant oscillations in the drag current, was caused by the coincidence of channel velocities of electrons near Fermi levels in two different wires.

Yu *et al.* [63] reported the electrical characterization of Si nanowire devices. Several types of device-crossed nanowire devices, 4 and 6 terminal devices and three-terminal (gated) devices were fabricated. Electrical contact to the wires (Schottky or Ohmic) and doping level controlled the wide variation of measured resistivity ranging from $\sim 10^5$ ohm-cm to $\sim 10^{-3}$ ohm-cm. Thermal diffusion of metal catalyst at 750–850°C was responsible for doping. Much larger solid solubility of Au in Si than Zn, resulted in reduction of resistivity in Au-nucleated wire in comparison to Zn-nucleated wires.

Li *et al.* [64] measured quantized conductance of metallic nanowires (Cu, Au) prepared by electrochemical etching a small region of metallic wire (width \sim micron) placed on a glass substrate down to the atomic scale. The width (hence conductance) of the nanowire, could be controlled by adjusting electrochemical potential-through etching-deposition-etching process. Using the feedback loop into the bipotentiostat, nanowires at preset conductance value could be synthesized in a fully automatic way. When the conductance value was lowered than the preset value, the potential was lowered to deposit the atoms back. When the conductance was greater, potential was increased to start etching. Nanowires having lifetime of several hours and preset conductance of integral multiples of $G_0 = 2e^2/h$ could be synthesized by the process. Nanowires with fractional conductance were found but they were unstable and changed to the structures of near interger conductance.

Pescini *et al.* [65] first measured low temperature conductivity of a novel device consisting of suspended Si nanowires. Nanowires were prepared by high-resolution, low-energy electron beam lithography and reactive ion etching in highly n-doped silicon film in silicon-on-insulator (SOI) substrates. Nanowires were made suspended by etching buried oxide layer under SOI using HF. I-V characteristic and differential conductivity measured at 2 K for 150 nm wire, showed nonlinear behavior near zero bias. This was explained by

random potential fluctuations present in highly doped Si nanostructure. The peaks appeared in the conductivity at ~ 0.17 mV of source to drain voltage was attributed to the presence of discrete phonon modes in the wires. An estimation of dominant phonon wavelength given by $\lambda_{\text{ph}} \approx V_s h / 2k_B T$ for $V_s = 9000$ mS $^{-1}$ at 2 K yielded $\lambda_{\text{ph}} \approx 110$ nm. Good agreement of λ_{ph} with the width and thickness of wires suggested the thermalphonon finite-size effect.

Cui *et al.* [66] used laser catalytic growth method to synthesize single crystal Phosphorus and Boron doped Silicon nanowires (SiNWs). A gold target was ablated by Nd: YAG laser to produce gold nanocluster as catalyst and SiH $_4$ was used as reactant. For Boron doping B $_2$ H $_6$ was added to reactant flow while for phosphorus doping Au-P target and red Phosphorus was used. For electrical measurement nanowires were supported on SiO $_2$ substrate with the underlying conducting Si used as a back gate. Al and Au contact were made by electron beam lithography. Two terminal, Gate voltage (V_g) dependent I-V characteristics, were recorded for intrinsic, Boron and Phosphorus doped SiNWs. Increase of conductance with increasing negative V_g indicated that SiNW was a p-type semiconductor. Similar and opposite V_g dependences were observed for B-doped and P-doped SiNW respectively. No V_g dependence with linear I-V data were recorded for heavily doped SiNWs. Doping could be controlled to reach a metallic regime (6.9×10^{-3} ohm-cm for B-doped and 2.3×10^{-2} ohm-cm for P-doped). Temperature dependent I-V data for heavily doped SiNWs showed no evidence for Coulomb blockade at temperature down to 4.2 K suggesting the structural and doping uniformity of SiNWs.

Lin *et al.* [67] proposed a semi-classical transport model to explain the temperature-dependent resistivity measurement on Bi nanowires as a function of wire diameter down to 7 nm. The model included anisotropic and nonparabolic carriers in cylindrical wires and various scattering processes, arising from wire boundary, grain boundary and ionized impurity. The model was extended for Te-doped (Te concentration 0–0.15 at%) 40 nm diameter Bi nanowires prepared by pressure injection technique.

Wong *et al.* [68] reported field-emission characteristics of SiC nanowires synthesized by hot filament chemical vapor deposition. Measurements were carried out in a vacuum chamber at a pressure $\sim 5 \times 10^{-8}$ Torr. A positive de voltage upto 5 kV was applied across the stainless steel anode and SiCNw films with separation of maximum 120 micron. Approximate exponential increase of emission current with the applied voltage was explained by Fowler-Nordheim theory [69]. Stability test of SiNw film at emission current density ~ 110 μ A/cm 2 for 3 h showed no degradation of current density.

Electrical property of individual vanadium pentoxide nanowires was measured by Muster *et al.* [70] V $_2$ O $_5$ fibers (length \sim few microns, height ~ 1.5 nm and width ~ 10 nm) were formed on aging the solution of ammonium (meta) vanadate in presence of acidic ion exchanger resin. Individual V $_2$ O $_5$ fibers were deposited on 3-aminopropyltriethoxysilane treated Si/SiO $_2$ sur-

faces and used for electrical characterization. Symmetric and nonlinear I-V characteristics with high resistance were observed for individual wires deposited on prefabricated electrodes. Lithographically deposited AuPd electrodes over V $_2$ O $_5$ fibers displayed lower resistance for both 2-probe and 4-probe measurements. Resistivity data in the temperature range 100–300 K was fitted with small polaron hopping model. Hopping was operative between V $^{4+}$ and V $^{5+}$ sites with activation energy of 0.11 eV.

Rapid charge transport along self-assembling graphitic nanowires was investigated by Craats *et al.* [71]. Charge transport properties were studied for hexakis-tetradecyl-BC (C14BC) and hexakis-hexylthio-triphenylene (HHTT) by using pulse-radiolysis time-resolved microwave conductivity technique (PR-TRMC). Sudden changes of one dimensional intercolumnar mobility with temperature were associated with several phase transitions of the nanowires.

Evans *et al.* [24] reported magnetotransport measurements of Co-Ni-Cu/Cu multilayered nanowires at 295 K and 77 K, using applied fields of up to 8 kOe, direction of field being perpendicular to the long axis of the wires. The recorded values of current perpendicular to plane giant magnetoresistance (CPP-GMR) were 55% at room temperature and 115% at 77 K for nominal layer thicknesses $t_{\text{Co-Ni-Cu}} = 54$ Å and $t_{\text{Cu}} = 21$ Å. This value was larger than the same system electrodeposited in track-etched polycarbonate membranes. Except for the smallest and largest t_{Cu} , the CPP-GMR for the annealed nanowires also exhibited the linear dependence predicted by the Valet-Fert model [72]. The use of aluminum oxide membranes also made possible a study of the effects of annealing on the CPP-GMR.

Duan *et al.* [73] investigated the detailed electrical and optoelectronic properties of assembly of functional nanoscale devices from indium phosphide nanowires. Single-crystal InP nanowires with n- and p-type doping were prepared by laser assisted catalytic growth method. Fig. 5a shows field-emission scanning electron microscopy images of the doped nanowires. In Fig. 5b and c the gate-dependent current-voltage characteristics for Te- and Zn-doped nanowires respectively are shown. Increase of conductance of Te-doped InP nanowire for increase of positive gate voltage confirmed that these nanowires were n-type. For Zn-doped InP nanowires an opposite trend was observed. Nanowires could be switched from off-state to on-state by controlling gate voltage, hence functioned as nanoscale field-effect transistors. Crossed wire p-n junctions exhibited rectifying behavior and also emitted light. Electroluminescence (EL) intensity increased sharply with bias voltage. Peak of the EL spectrum (820 nm) was blue shifted relative to bulk (925 nm) InP. Thus smallest light-emitting diode with junction diameters 39 nm \times 49 nm was fabricated. Electric-field-directed assembly of nanowires was constructed for highly integrated device.

Huang *et al.* [74] fabricated Logic Gates using crossed nanowire p-n junctions. Junction arrays with controllable electrical characteristics were used to

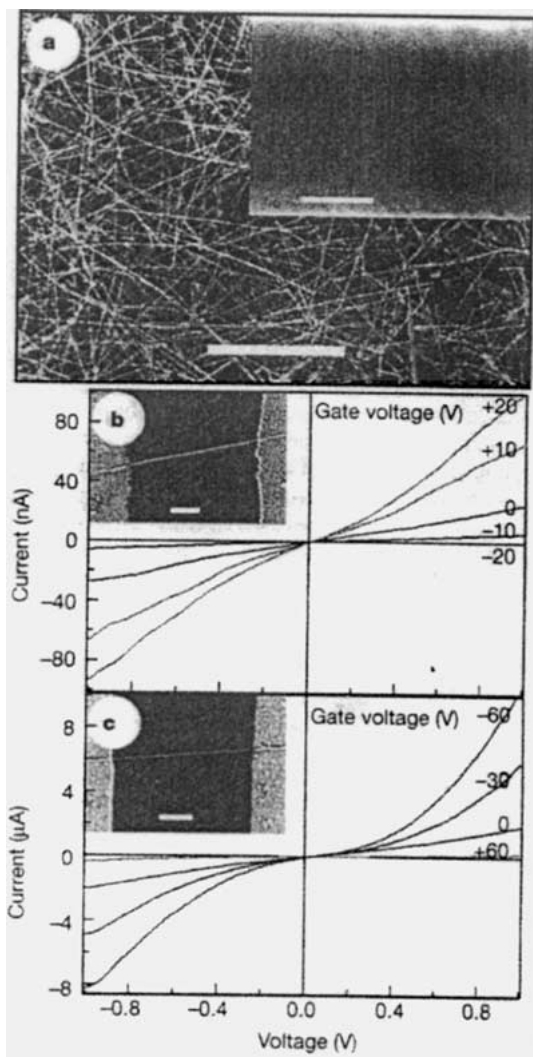


Figure 5 (a) Field-emission scanning electron microscopy image of Zn-doped InP nanowires. (b) Gate-dependent current-voltage behaviour for Te-doped InP nanowire. (c) Gate-dependent current-voltage behaviour for Zn-doped InP nanowire. (Reprinted by permission from Xiangfeng Duan, Yu Huang, Yi Cui, Jiangfang Wang and C. M. Lieber, *Nature* **409** (2001) 66. Copyright (2001), Macmillan Magazines Ltd.)

construct integrated nanoscale field-effect transistors. Nanowire junction arrays were used for basic logic gates OR, AND and NOR.

He *et al.* [33] studied conductance jumps for stretched polyaniline nanowires synthesized by electrochemical polymerization of aniline onto a sharp scanning tunneling microscope tip. The conductance was shown to initially increase due to alignment of polymer chains by stretching followed by a stepwise decrease due to abrupt changes of the nanowire diameter. By changing the electrochemical potential it was observed that the current-voltage behaviour changed from ohmic to rectifying characteristics.

Lau *et al.* [75] measured the temperature dependence of resistance for different superconducting nanowires having widths ranging from 10 to 22 nm and lengths varying from 100 nm to 1 μm. Amorphous $\text{Mo}_{0.79}\text{Ge}_{0.29}$ nanowires were fabricated by sputtering onto carbon nanotubes suspended across slits on $\text{SiN}/\text{SiO}_x/\text{Si}$ substrates. Observations of increasingly broad resistivity transitions with decreasing cross sectional areas were explained by thermally activated

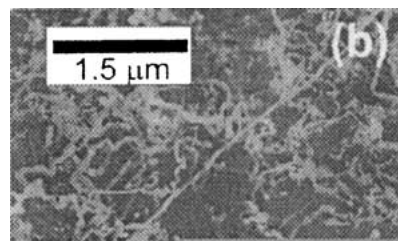


Figure 6 Scanning electron micrograph for Ge nanowires prepared by vapour-liquid-solid growth mechanism (Reprinted by permission from G. Gu, M. Burghard, G. T. Kim, G. S. Dusberg, P. W. Chiu, V. Kristic, S. Roth, W. Q. Han, *Journal of Applied Physics* **90** (2001) 5747. Copyright (2001), American Institute of Physics).

phase slips close to T_c and quantum phase slips at low temperatures.

Gu *et al.* [76] synthesized single crystalline Ge nanowires with diameters in the range 20 to 180 nm from gold nanoparticles based on a vapour-liquid-solid growth mechanism. Fig. 6 is a scanning electron micrograph of Ge nanowires. Transport measurements were carried out on individual nanowires which indicated that they were heavily doped during growth. The electrical resistivity data were explained by the thermal fluctuation tunneling conduction model.

7. Summary

Nanowires of metals, semiconductors and polymers have been synthesized by various workers. The methods of preparation have been chemical, electrodeposition, physical and carbon nanotube filling. Quantum effects have been observed in the transport properties of many of these nanowires. Nanodevice and nanojunctions have also been formed in several systems. These hold promise for the miniaturization of electron devices.

References

1. J. R. HEATH, *Science* **270** (1995) 1315.
2. A. P. ALIVISATOS, *ibid.* **271** (1996) 933.
3. R. P. ANDRES, J. D. BIELEFELD, J. I. HENDERSON, D. B. JANES, V. R. KOLAGUNTA, C. P. KUBIAK, W. J. MAHONEY and R. G. OSIFCHIN, *ibid.* **273** (1996) 1690.
4. R. LANDANER, *J. Phys.: Condens. Mater* **1** (1989) 8099.
5. Y. IMRY, in "Nanostructures and Mesoscopic Systems," edited by W. P. Kirk and M. A. Reed (Academic, New York, 1992) p. 11.
6. A. J. COX, J. G. LOUDERBACK and L. A. BLOOMFIELD, *Phys. Rev. Lett.* **71** (1993) 923.
7. R. F. PEASE, in "Nanostructures and Mesoscopic Systems," edited by W. P. Kirk and M. A. Reed (Academic, New York, 1992) p. 37.
8. H. J. BLYTHE, V. M. FEDOSYK, O. I. KASYUTICH and W. SCHWARZACHER, *J. Magn. Magn. Mater.* **208** (2000) 251.
9. S. T. LEE, Y. F. ZHANG, N. WANG, Y. H. TANG, I. BELLO, C. S. LEE and Y. W. CHUNG, *J. Mater. Res.* **14** (1999) 4503.
10. J. R. HEATH and F. K. LEGOUES, *Chem. Phys. Lett.* **208** (1993) 263.
11. C. A. HUBER, T. E. HUBER, M. SADOQI, J. A. LUBIN, S. MANALIS and C. B. PRATER, *Science* **263** (1994) 800.
12. T. J. TRENTLER, K. M. HICKMAN, S. C. GOEL, A. M. VIANO, P. C. GIBBONS and W. E. BUHRO, *ibid.* **270** (1995) 1791.
13. J. D. HOLMES, K. P. JOHNSTOM, R. C. DOTY and B. A. KORGEL, *ibid.* **287** (2000) 1417.
14. Y.-J. HAN, J. M. KIM and G. D. STUCKY, *Chem. Mater.* **12** (2000) 2068.

15. D. ZHAO, J. FENG, Q. HUO, N. MELOSH, G. H. FREDRICKSON, B. F. CHMELKA, G. D. STUCKY, *ibid.* **279** (1998) 548.
16. S. WANG and S. YANG, *Chem. Phys. Lett.* **322** (2000) 567.
17. G. W. MENG, Z. CUI, L. D. ZHANG and F. PHILLIPP, *J. Cryst. Growth* **209** (2000) 801.
18. J. Q. HU, Q. Y. LU, K. B. TANG, B. DENG, R. R. JIANG, Y. T. QIAN, W. C. YU, G. E. ZHOU, X. M. LIU and J. X. WU, *J. Phys. Chem. B* **104** (2000) 5251.
19. B. GATES, Y. YIN and Y. XIA, *J. Am. Chem. Soc.* **122** (2000) 12582.
20. N. R. B. COLEMAN, M. A. MORRIS, T. R. SPALDING and J. D. HOLMES, *ibid.* **123** (2001) 187.
21. J. ZHAN, X. YANG, D. WANG, S. LI, Y. XIE, Y. XIA and Y. QIAN, *Adv. Mater.* **12** (2000) 1348.
22. T. BJORNHOLM, T. HASSENKAM, D. R. GREVE, R. D. MCCULLOUGH, M. JAYARAMAN, S. M. SAVOY, C. E. JONES and J. T. MCDEVITT, *ibid.* **11** (1999) 1218.
23. L. SUN, P. C. SEARSON and C. L. CHIEN, *Appl. Phys. Lett.* **74** (1999) 2803.
24. P. R. EVANS, G. YI and W. SCHWARZACHER, *ibid.* **76** (2000) 481.
25. G. FASOL and K. G. RUGE, *ibid.* **70** (1997) 2467.
26. D. XU, X. SHI, G. GUO, L. GUI and Y. TANG, *J. Phys. Chem. B* **104** (2000) 5061.
27. S.-J. CHOI and S.-M. PARK, *Adv. Mater.* **12** (2000) 1547.
28. S. BHATTACHARYYA, S. K. SAHA and D. CHAKRAVORTY, *Appl. Phys. Lett.* **76** (2000) 3896.
29. *Idem.*, *ibid.* **77** (2000) 3770.
30. A. DAN and D. CHAKRAVORTY, unpublished.
31. H. CAO, Z. XU, H. SANG, D. SHENG and C. TIE, *Adv. Mater.* **13** (2001) 121.
32. S. A. SAPP, B. B. LAKHSMI and C. R. MARTIN, *ibid.* **11** (1999) 402.
33. H. X. HE, C. Z. LI and N. J. TAO, *Appl. Phys. Lett.* **78** (2001) 811.
34. Y. KONDO and K. TAKAYANAGI, *Science* **289** (2000) 606.
35. Z. G. BAI, D. P. YU, H. Z. ZHANG, Y. DING, Y. P. WANG, X. Z. GAI, Q. L. HANG, G. C. XIONG and S. Q. FENG, *Chem. Phys. Lett.* **303** (1999) 311.
36. D. P. YU, Z. G. BAI, Y. DING, Q. L. HANG, H. Z. ZHANG, J. J. WANG, Y. H. ZOU, W. QIAN, G. C. XIONG, H. T. ZHOU and Q. S. FENG, *Appl. Phys. Lett.* **72** (1998) 3458.
37. H. F. YAN, Y. J. XING, Q. L. HANG, D. P. YU, Y. P. WANG, J. XU, Z. H. XI and S. Q. FENG, *Chem. Phys. Lett.* **323** (2000) 224.
38. H. Y. PENG, X. T. ZHOU, N. WANG, Y. F. ZHENG, L. S. LIAO, W. S. SHI, C. S. LEE and S. T. LEE, *ibid.* **327** (2000) 263.
39. Y. C. CHOI, W. S. KIM, Y. S. PARK, S. M. LEE, D. J. BAE, Y. H. LEE, G.-S. PARK, W. B. CHOI, N. S. LEE and J. M. KIM, *Adv. Mater.* **12** (2000) 746.
40. Y. F. ZHANG, Y. H. TANG, N. WANG, D. P. YU, C. S. LEE, I. BELLO and S. T. LEE, *Appl. Phys. Lett.* **72** (1998) 1835.
41. Y. H. TANG, Y. F. ZHANG, H. Y. PENG, N. WANG, C. S. LEE and S. T. LEE, *Chem. Phys. Lett.* **314** (1999) 16.
42. X. DUAN and C. M. LIEBER, *Adv. Mater.* **12** (2000) 298.
43. C. H. LIANG, G. W. MENG, L. D. ZHANG, N. F. SHEN and X. Y. ZHANG, *J. Cryst. Growth* **218** (2000) 136.
44. A. K. SINHA, D. W. HWANG and L.-P. HWANG, *Chem. Phys. Lett.* **332** (2000) 455.
45. C. KIANG, J. CHOI, T. TRAN and A. BACHER, *J. Phys. Chem. B* **103** (1999) 7449.
46. A. RUBIO, J. L. CORKILL and M. L. COHEN, *Phys. Rev. B* **53** (1996) 4023.
47. N. G. CHOPRA *et. al.*, *Science* **269** (1995) 966.
48. W. HAN, S. FAN, Q. LI and Y. HU, *Science* **277** (1997) 1287.
49. A. D. BERRY, R. J. TONUCCI and M. FATEMI, *Appl. Phys. Lett.* **69** (1996) 2846.
50. A. BEZRYADIN, C. N. LAU and M. TINKHAM, *Nature* **404** (2000) 971.
51. D. N. DAVYDOV, J. HARUYAMA, D. ROUTKEVITCH, B. W. STATT, D. ELLIS, M. MOSKOVITS and J. M. XU, *Phys. Rev. B* **57** (1998) 13550.
52. Y. V. NAZAROV, *Sov. Phys. JETP* **68** (1989) 561.
53. *Idem.*, *JETP Lett.* **49** (1989) 126.
54. D. NATELSON, R. L. WILLETT, K. W. WEST and L. N. PFEIFFER, *Solid. State. Commun.* **115** (2000) 269.
55. S. KANJANACHUCHAI, T. J. THORNTON, J. M. FERNÁNDEZ and H. AHMED, *Semicond. Sci. Technol.* **16** (2001) 72.
56. S.-W. CHUNG, J.-Y. YU and J. R. HEATH, *Appl. Phys. Lett.* **76** (2000) 2068.
57. F. D. M. HALDANE, *J. Phys. C: Solid State Phys.* **14** (1981) 2585.
58. H. J. SCHULTZ, *Phys. Rev. Lett.* **71** (1993) 1864.
59. S. M. GIRVIN, L. I. GLAZMAN, M. JONSON, D. R. PENN and M. D. STILES, *Phys. Rev. Lett.* **64** (1990) 3183.
60. K. A. MATVEEV, D. YUE and L. I. GLAZMAN, *ibid.* **71** (1993) 3351.
61. S. V. Z-ZOTOV, Y. A. KUMZEROV, Y. A. FIRSOV and P. MONCEAU, *J. Phys: Condens. Mater.* **12** (2000) L303.
62. V. L. GUREVICH, V. B. PEVZNER and E. W. FENTON, *ibid.* **10** (1998) 2551.
63. J.-Y. YU, S.-W. CHUNG and J. R. HEATH, *J. Phys. Chem. B* **104** (2000) 11864.
64. C. Z. LI, A. BOGOZI, W. HUANG and N. J. TAO, *Nanotechnology* **10** (1999) 221.
65. L. PESCHINI, A. TILKE, R. H. BLICK, H. LORENTZ, J. P. KOTTHAUS, W. EBERHARDT and D. KERN, *ibid.* **10** (1999) 418.
66. Y. CUI, X. DUAN, J. HU and C. M. LIEBER, *J. Phys. Chem. B* **104** (2000) 5213.
67. Y.-M. LIN, S. B. CRONIN, J. Y. YING, M. S. DRESSELHAUS and J. P. JEREMANS, *Appl. Phys. Lett.* **76** (2000) 3944.
68. K. W. WONG, X. T. ZHOU, F. C. K. AU, H. L. LAI, C. S. LU and S. T. LU, *ibid.* **75** (1999) 2918.
69. R. H. FOWLER and L. W. NORDHEIM, *Proc. R. Soc. London, Ser. A* **119** (1928) 173.
70. J. MUSTER, G. T. KIM, V. KRSTIC, J. G. PARK, Y. W. PARK, S. ROTH and M. BURGHARD, *Adv. Mater.* **12** (2000) 420.
71. A. M. CRAATS, J. M. WARMAN, K. MÜLLEN, Y. GEERTS and J. D. BRAND, *Adv. Mater.* **10** (1998) 36.
72. T. VALET and A. FERT, *Phys. Rev. B* **48** (1993) 7099.
73. X. DUAN, Y. HUANG, Y. CUI, J. WANG and C. M. LIEBER, *Nature* **409** (2001) 66.
74. Y. HUANG, X. DUAN, Y. CUI, L. J. LUAHON, K.-H. KIM and C. M. LIEBER, *Science* **294** (2001) 1313.
75. C. N. LAU, N. MARKOVIC, M. BOCKRATH, A. BEZRYADIN and M. TINKHAM, *Phys. Rev. Lett.* **87** (2001) 217003.
76. G. GU, M. BURGHARD, G. T. KIM, G. S. DUSBERG, P. H. CHIU, V. KRSTIC, S. ROTH and W. Q. HAN, *J. Appl. Phys.* **40** (2001) 5747.

Received 15 February
and accepted 23 May 2002